Advection-condensation paradigm for stratospheric water vapor

Y. S. Liu,[1,2] S. Fueglistaler,[1,3] and P. H. Haynes[1]

Received 13 April 2010; revised 20 September 2010; accepted 28 September 2010; published 21 December 2010.

[1] The advection-condensation (A-C) paradigm is a starting point for a theoretical framework for analysis of atmospheric water vapor distributions and changes therein in a changing climate. It postulates that water vapor concentrations are governed to leading order by the transport through the full four-dimensional temperature (and hence saturation mixing ratio) field. Brewer's (1949) qualitative deduction of the stratospheric circulation based on water vapor measurements was a first and prominently successful application of this paradigm. Here we examine the quantitative validity of the A-C paradigm by predicting stratospheric water vapor based on the saturation mixing ratio at the Lagrangian dry point of trajectories calculated using data from the European Centre for Medium-range Weather Forecasts. Using different data sets for the calculation, we show that results are sensitive to seemingly small differences in temperatures and wind fields and that interpretation of results (in terms of identification of effects of processes deliberately neglected by the advection-condensation paradigm) requires a careful error calculation. We introduce a semiempirical approach to analyze errors in the Lagrangian predictions of water vapor. We show that persistent (in time and space) errors in the temperature fields lead to similar errors in the Lagrangian model predictions. Conversely, biases in the *variance* of the temperature fields introduces a systematic *bias* in the model prediction. Further, model predictions are affected by dispersion and the time scale of troposphere-to-stratosphere transport. Our conclusion is that water vapor predictions for the stratospheric overworld based on the A-C paradigm have a dry bias of −40% ± 10% and −50% ± 10% when small-space-scale and short-time-scale temperature fluctuations not resolved by the ECMWF reanalyses are taken into account. We suggest that the correction to the A-C paradigm most likely to remove this dry bias is the inclusion of cloud microphysical processes (such as incomplete sedimentation of particles allowing reevaporation), which relax the assumption of instantaneous dehydration to the saturation mixing ratio. Interestingly, the bias attributed to the A-C paradigm in terms of water vapor concentration is found to be proportional to the measured water concentration, and a constant offset in terms of frost point temperature can account for much of the bias and its variability in water vapor mixing ratios.

Citation: Liu, Y. S., S. Fueglistaler, and P. H. Haynes (2010), Advection-condensation paradigm for stratospheric water vapor, *J. Geophys. Res.*, *115*, D24307, doi:10.1029/2010JD014352.

1. Introduction

[2] The strong temperature dependence of water vapor pressure, in conjunction with the atmosphere's temperature structure, leads to an atmospheric water vapor distribution that is strongly controlled by transport processes or, more precisely, by the advection through the atmospheric saturation mixing ratio field. This is particularly clear for stratospheric water vapor, where this property allowed *Brewer* [1949] to deduce the general circulation in the stratosphere from only a few water vapor observations. The notion that transport through the atmosphere's saturation mixing ratio field can be seen as the leading order process controlling atmospheric water vapor distributions is often described as the "advection-condensation" (A-C) paradigm [*Pierrehumbert and Roca*, 1998].

[3] Here, we analyze the relationship between transport and atmospheric water vapor in the context of troposphere-to-stratosphere transport (TST). We argue that the upper troposphere/lower stratosphere region provides an ideal context to analyze the relation between atmospheric water vapor and transport. Indeed the relation between the two may provide novel insights into aspects of TST such as the relative importance between diabatic transport into the strato-

[1]Department of Applied Mathematics and Theoretical Physics, University of Cambridge, Cambridge, UK.
[2]Now at School of Mathematics and Statistics, University of St Andrews, Saint Andrews, UK.
[3]Now at Department of Geosciences, Princeton University, Princeton, New Jersey, USA.

0148-0227/10/2010JD014352

spheric overworld and quasi-isentropic transport into the lowermost stratosphere (using terminology following *Hoskins* [1991]; *Holton et al.* [1995]).

[4] Previous work [*Fueglistaler et al.*, 2005; *Fueglistaler and Haynes*, 2005] has shown generally good agreement between model predictions based on trajectory calculations and observed stratospheric water vapor, but we show here that results are more sensitive to details in the model calculations than previously thought. Consequently, assessment of the validity of the A-C paradigm and indeed improving on that paradigm requires a thorough analysis of the sensitivity of model results to errors in the underlying temperature field and the representation of transport. Here, we introduce a semiempirical approach to this challenging problem. The insights obtained here for the specific case of stratospheric water vapor from a Lagrangian perspective are also applicable to the corresponding problem in the troposphere and to the interpretation of water vapor fields calculated in a conventional Eulerian global circulation model.

[5] We explore the relation between transport and atmospheric water vapor using trajectory calculations. The water vapor concentration of each trajectory is determined from the minimum saturation mixing ratio encountered prior to observation. The point at which the minimum occurs will be called the Lagrangian dry point (LDP), where each LDP has an associated time, position, pressure, temperature, and saturation mixing ratio. The A-C paradigm postulates that the atmospheric water vapor distribution can be predicted by the properties of the LDP distribution. (Note that the LDP is in most cases identical with the "Lagrangian cold point" [*Fueglistaler et al.*, 2004], but we introduce the new term LDP here to encourage precision.)

[6] Trajectories are calculated with data from two different reanalyses carried out at the European Centre for Medium-range Weather Forecasts (ECMWF), namely the widely used ERA-40 [*Uppala et al.*, 2005] and the more recent interim reanalysis at ECMWF, called ERA-Interim [*Simmons et al.*, 2006; *Uppala et al.*, 2008; *Fueglistaler et al.*, 2009b]. These two data sets are arguably among the best available reconstructions of atmospheric temperature and circulation. In each case we carry out two sets of trajectory calculations: kinematic trajectories based on the three components of the wind field and diabatic trajectories based on the two horizontal wind components combined with model diabatic heating rates. Hence, we have four slightly different representations of transport, which allows us to study the role of relatively small differences in transport on the predicted water vapor field. Numerous studies have emphasized that kinematic trajectories tend to be too dispersive [e.g., *Schoeberl*, 2004; *Stohl et al.*, 2004; *Wohltmann and Rex*, 2008]. It has also been shown that the results from modeling of thin tropical cirrus are substantially improved when using diabatic heating rates [*Immler et al.*, 2007]. However, it remains to be shown whether all aspects of transport derived from diabatic trajectory calculations are always more accurate since, for example, errors in the model's diabatic terms (unconstrained by observations, see e.g., *Fueglistaler et al.* [2009b]) can lead to erroneous representation of transport.

[7] It is to be understood that the A-C paradigm by itself does not necessarily imply neglect of atmospheric mixing processes. Some methods to evaluate the A-C paradigm allow direct incorporation of mixing effects [e.g., *Galewsky et al.*, 2005; *Wright et al.*, 2010] at the cost of loss of information about transport pathways. Trajectory-based calculations as used here cannot take into account the effect of mixing on the water vapor mixing ratio for an individual trajectory. However, the results we show are averages over large ensembles of trajectories (which may be local averages) and in that sense account for the effect of mixing in the subsaturated stratosphere. (There could in principle be a more subtle effect of mixing in the dehydration region itself, but for the purpose of this paper we take the view that other sources of error need to be considered first.)

[8] In the following, we first discuss in section 2 the situation of the upper troposphere/lower stratosphere from the perspective of water vapor. Section 3 describes data and methods, and section 4 compares stratospheric water vapor concentrations from model predictions with observations. Section 5 presents an analysis of errors arising from the method to evaluate the A-C paradigm, allowing a quantification of the effect of physical processes deliberately neglected in the A-C paradigm. Finally, section 6 provides a discussion of the implications of our results.

2. Circulation, Vapor Pressure, and Observed Water Vapor Distribution in the Lower Stratosphere

[9] In the stratosphere, the dynamically forced meridional overturning circulation forces the temperature away from radiative equilibrium, yielding a region of radiative heating at low latitudes and radiative cooling at high latitudes.

[10] Figure 1 shows the mean position of the surface separating radiative ascent from descent (the black line; determined from ERA-Interim radiative transfer calculations; see *Fueglistaler et al.* [2009b]), superimposed on the mean saturation mixing ratio field. The saturation mixing ratio field essentially mirrors the mean temperature structure, with the near exponential (i.e., $\exp(-1/T)$) temperature dependence of the water vapor pressure. In the tropics, this leads to a decrease in the water vapor pressure of about 5 orders of magnitude from the ground to the tropopause. The corresponding decrease in saturation mixing ratio is 4 orders of magnitude due to the associated decrease in pressure. In the lower stratosphere temperature increases with height, and, correspondingly, the saturation mixing ratio also increases rapidly. In addition to the vertical gradient, the variations in saturation mixing ratio on sloping isentropes (up to 2 orders of magnitude for isentropes around 300 K potential temperature) are of importance.

[11] Comparison of the saturation mixing ratio field (Figure 1a) with observed water vapor mixing ratios (Figure 1b) shows large differences, pointing to a key role of the circulation through the temperature field. It is this striking discrepancy, particularly in the extratropics between the local saturation mixing ratio field and observed water vapor mixing ratios, that allowed *Brewer* [1949] to deduce the general circulation of the stratosphere.

[12] Within the stratosphere, the increase in saturation mixing ratio relative to the values around the tropical tropopause renders water vapor essentially a passive tracer, with the exception of dehydration in the Southern polar winter, and a chemical source from methane oxidation. The latter is

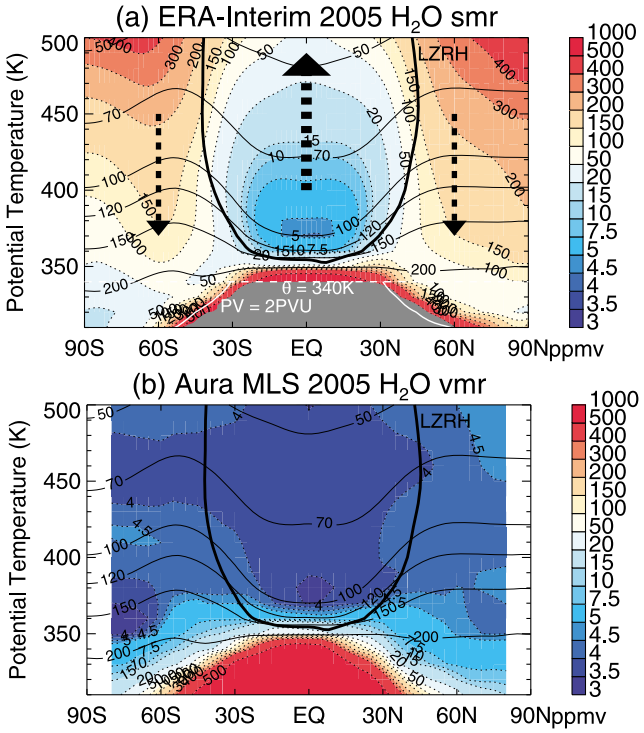

Figure 1. (a) The annual mean (year 2005) zonal mean structure of the lower stratospheric saturation mixing ratio (color coded) in an isentropic coordinate system. The black lines show isobars (200/150/120/100/70/50 hPa, as labeled). The white line shows the 2 PVU surface, used in conjunction with the 340 K isentrope (white dashed line) and the condition that saturation mixing ratio exceeds 1000 ppmv (giving the gray shaded area) to identify troposphere-to-stratosphere transport (see text). The black bold line shows where clear sky radiative heating is zero. Black dashed arrows show schematically the diabatic residual circulation. (b) The corresponding observed water vapor distribution from Microwave Limb Sounder on board the Aura satellite.

important higher up in the stratosphere, and consequently stratospherically older air is moister than at entry.

[13] The stratospheric overworld (above about 380 K potential temperature) may be reached only by cross-isentropic transport, while the extratropical lowermost stratosphere may be reached either by diabatic subsidence from the overworld or quasi-isentropically from the tropical troposphere. Cross-isentropic transport from the troposphere into the stratospheric overworld necessarily passes through the region of minimum saturation mixing ratios around the tropical tropopause. Quasi-isentropic transport can bring substantially moister air into the extratropical lowermost stratosphere, but given the pattern of dynamically forced diabatic ascent and descent, these air masses may never reach higher stratospheric levels. The surface separating regions of ascent and descent (its lower bound is often termed the "level of zero radiative heating," LZRH) is an important aspect of the circulation that needs to be considered alongside the well-established concepts of overworld and lowermost stratosphere.

[14] The observed water vapor mixing ratios in the lowermost stratosphere (Figure 1b; and similarly ozone concentrations, not shown) suggest that quasi-isentropic transport must in practice be limited, and indeed the region of the subtropical jets is known to be a "transport barrier" (which can be clearly seen, for example, in the calculations of effective diffusivity by *Haynes and Shuckburgh* [2000]).

3. Data and Methods

[15] We calculate domain-filling kinematic trajectories using the OFFLINE trajectory code [*Methven*, 1997; *Methven et al.*, 2003], where the vertical velocity at each time step is obtained by solving the continuity equation. The diabatic trajectories are calculated using a modified version of the OFFLINE code [*Liu*, 2009]. In this modified version of the code, the vertical motion is calculated using heating rates, which are the time-averaged accumulated potential temperature tendencies in the model over a fixed time period (normally 6 h). At each time step for each individual trajectory, we interpolate from ECMWF η coordinates (a sigma-pressure hybrid) to potential temperature coordinates, calculate the new vertical position using the heating rate information, and then reinterpolate to η coordinates. Trajectories are started on a 2°/2° longitude/latitude grid. For comparison of time series with measurement, trajectories are started once per month at 82 hPa, whereas for analysis of the latitude-height structure trajectories are started on isentropic levels every 10 K between 310 K and 450 K. The integration period is chosen sufficiently long (up to 1 year; discussed below) to ensure that a substantial fraction of trajectories can be traced back to the troposphere. Overall, the number of 1 year trajectories analyzed for this study is of order 10^7, with an additional 10^7 trajectories with a 5 month integration period.

[16] Trajectories classified as "stratospheric" must satisfy the following conditions at their end points: the absolute value of potential vorticity (PV) must be larger than 4 potential vorticity units (PVU)(1 PVU = 10^{-6} km^2 kg^{-1} s^{-1}) or the potential temperature must be greater than or equal to 370 K. The 4 PVU criterion is a conservative criterion (commonly, the tropopause is located near 2 to 3 PVU) to minimize effects from spurious short-term troposphere-stratosphere exchange. The choice of 370 K (rather than the more conventional 380 K) as potential temperature criterion simply reflects the fact that the cold point tropopause is often a little lower than 380 K; other than showing slightly more data in Figure 3 this choice has no impact on conclusions of this study.

[17] The objective is to predict water vapor distributions governed by transport through the temperature field, and as such care must be taken that the predicted fields are independent of initial conditions. Therefore, we apply the following criteria to identify trajectories representing "troposphere-to-stratosphere transport" (subsequently termed the "TST ensemble"). In addition to the requirement that the back trajectories' start point lies in the stratosphere (as defined above), we require that they are traceable to a region where (i) potential vorticity is less than 2 PVU, (ii) potential temperature is less or equal to 340 K, and (iii) the saturation mixing ratio is larger than 1000 ppmv. The latter value is about 2 orders of magnitude larger than mixing ratios in the stratosphere, and hence any information of the water vapor initial condition is eliminated during transport into the

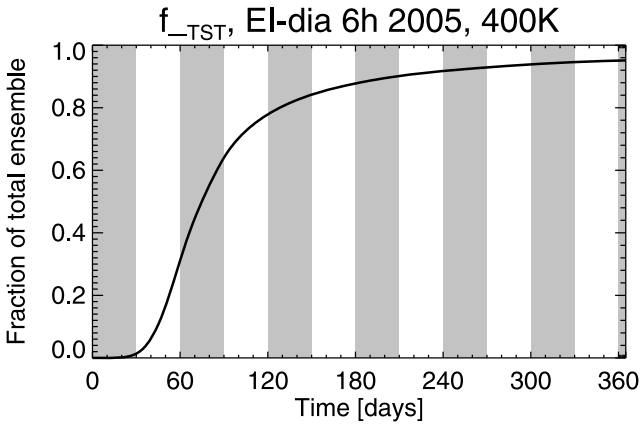

Figure 2. Cumulative distribution of transit time from the tropospheric source condition (see text) to 400 K for trajectories ending between 30°S and 30°N for the year 2005.

stratosphere. In addition to results based on the TST ensemble, results using all trajectories will be shown where needed, with additional information about methods given in the text.

[18] Water vapor concentrations are calculated from the LDP (i.e., are set to the minimum saturation mixing ratio encountered along the trajectory). Trajectories are calculated using ERA-40 and ERA-Interim data. In each case we use both the three-dimensional wind fields (kinematic trajectories) and horizontal wind fields combined with the model diabatic heating rates (diabatic trajectories). Hence, we get four sets of calculations, subsequently also termed "models": E40-kin, E40-dia, EI-kin, and EI-dia. As stated in the introduction, diabatic trajectories are found to be less dispersive than kinematic (though, as will be shown below, the difference is much reduced for ERA-Interim). This is because the available, instantaneous vertical wind field is far more noisy than the diabatic heating rates (also, the diabatic heating rates used here are averages over 6 h).

[19] The reanalysis data are available every 6 h, and it has been emphasized before that a higher temporal resolution of the input may improve the results. We find that increasing the temporal resolution of the input fields is for ERA-Interim a second-order effect compared to the differences between the four models. Hence, we present in this paper results derived only from input fields taken every 6 h.

[20] The length of the trajectory integration is known to affect results [*Bonazzola and Haynes*, 2004]. Consequently, we have used 1 year integration periods whenever possible; due to technical limitations some calculations had to rely on 5 month integration periods. The fraction of trajectories that can be traced back to the troposphere (the TST ensemble) depends on position in the stratosphere and trajectory method (i.e., kinematic versus diabatic).

[21] Figure 2 shows that at 400 K potential temperature in the tropics, the TST fraction is typically larger than 90% for 1 year and larger than 70% for 5 month integration periods. We found that results agree in general with the anticipated sensitivity to integration length. For example, the longer the integration period is, the longer is the mean time to travel from troposphere to the stratosphere, and the smaller is the amplitude of seasonal variations because of averaging over out-of-phase LDP temperatures.

[22] Model predictions of stratospheric water vapor are compared against measurements by the Microwave Limb Sounder on board the Aura satellite (MLS/Aura). We screened this data following the recommendations given by *Read et al.* [2007] and *Lambert et al.* [2007]. Because of lack of temporal overlap between ERA-40 and MLS/Aura, we carry out the model intercomparison for the year 2001, and results from calculations using ERA-Interim are compared to measurements from the MLS/Aura instrument with a focus on the year 2005.

4. Water Vapor Predictions

[23] In this section, we first show the water vapor field based on the LDP of the TST ensemble for all four model calculations. In a second step, a simple conceptual model is applied to estimate the water vapor of the non-TST trajectories and the contribution from methane oxidation, and the resulting water vapor field is compared to observations.

4.1. Water Vapor Predictions Based on the TST Ensemble

[24] Figure 3 shows the calculated water vapor mixing ratios in the stratosphere of the TST ensemble of 5-month back-trajectories, plotted as function of potential temperature. Figure 3 shows that the kinematic trajectory calculations using ERA-40 (E40-kin) yield results very different from the other three models. In particular, E40-kin shows much higher water vapor values above about 360 K. Closer inspection further shows that the two diabatic model calculations (E40-dia and EI-dia) yield lower water vapor mixing ratios in the stratosphere below 350K than the kinematic model calculations with either ERA-40 or ERA-Interim winds.

[25] The fractions of trajectories that can be traced back to the troposphere (TST fraction, white contour lines) within the 5 month integration period also show marked differences between the four model calculations. In particular, it is again the E40-kin model calculation that stands out with a much larger TST fraction at higher latitudes and/or higher altitudes than the three other models.

[26] The pronounced differences in the predicted water vapor field (in particular between E40-kin and the other three calculations) confirm that water vapor is a sensitive tracer of transport, but that this very sensitivity also can seriously distort model predictions. Attribution of differences in predicted water vapor to differences in temperatures and transport requires a thorough error discussion. In the following, we first compare the model predictions with measurements to obtain an overview of their overall quality and then present the error discussion.

4.2. Comparison With MLS/Aura Measurements

[27] The water vapor field based on the TST ensemble cannot be directly compared to measurements because it does not include the contribution from methane oxidation. Moreover, because of the long tail in the age distribution of stratospheric air, there will be a fraction of trajectories that cannot be traced back to the troposphere within a given length of integration. For the following comparison, we will use 1 year back-trajectories (i.e., substantially longer than the 5 month trajectories used for Figure 3), and will show

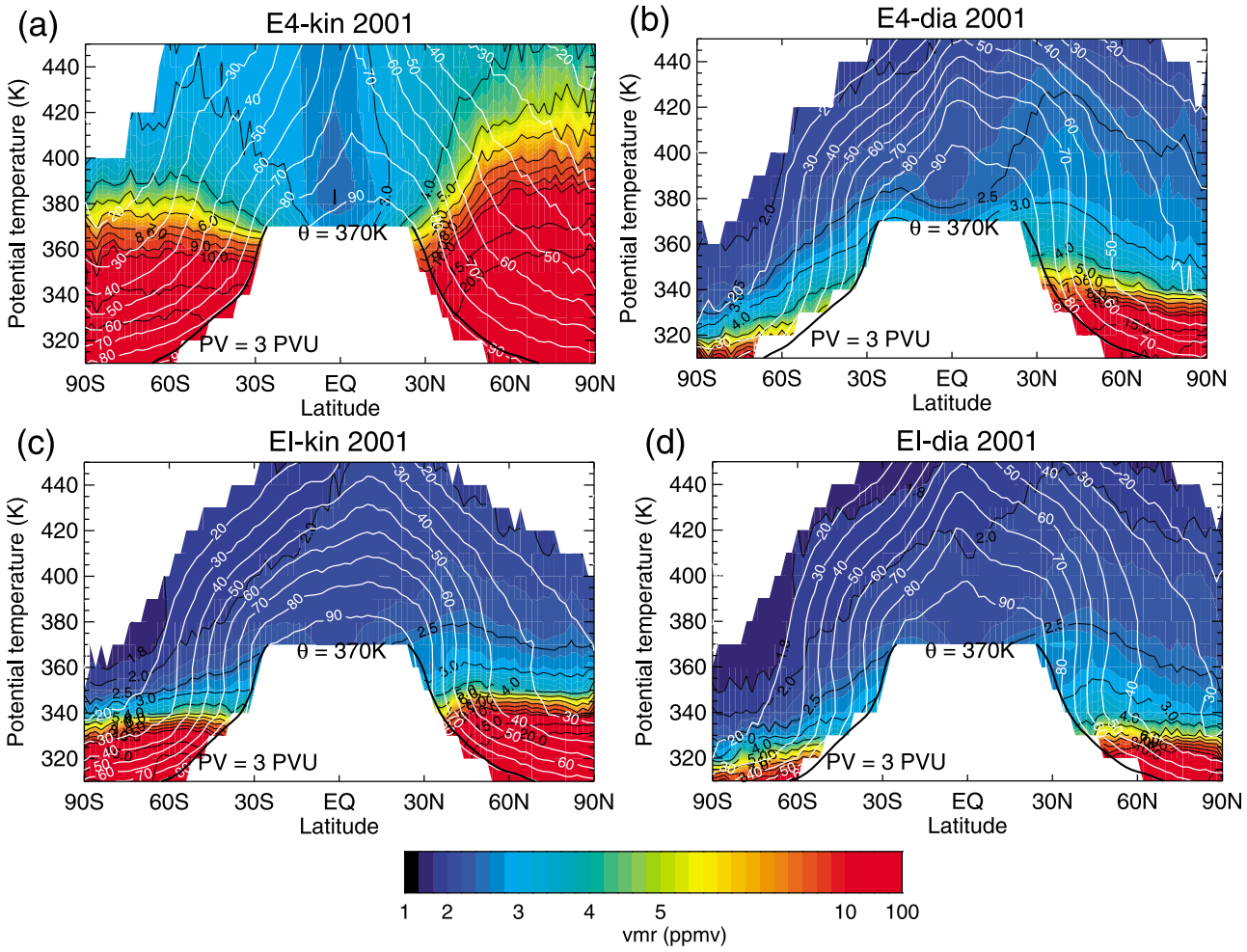

Figure 3. Annual mean (2001) stratospheric (here defined as having potential temperature larger than 370 K or potential vorticity larger than 4 PVU) water vapor concentrations calculated from those trajectories that can be traced back to the troposphere (the TST ensemble, see text). (a) ERA-40, kinematic trajectories; (b) ERA-40, diabatic trajectories; (c) ERA-Interim, kinematic trajectories; (d) ERA-Interim, diabatic trajectories. The white contour lines show the fraction (in percentages, as labeled) of trajectories that can be traced back to the troposphere within 5 months. The black line shows the climatological mean position of the 3 PVU surface for reference.

results only for regions where the TST fraction is larger than 35% (changing this threshold mainly affects the size of the domain, and does not affect conclusions).

[28] In order to allow clear identification of model shortcomings, we do not estimate mixing ratios of non-TST trajectories based on measurements in the region of origin (as done, e.g., in *Fueglistaler et al.* [2005]). Instead, we set their water vapor to entry mixing ratios of stratospherically older air masses as estimated by the model. To do so, we take the tropical mean (20°S–20°N) at 400 K potential temperature as a proxy for entry mixing ratios, whereby we account for the fact that the previous year (2004) was drier (see Figure 6 below) by reducing the mean value of 2005 by 0.15 ppmv.

[29] We further assume that the contribution from methane oxidation during the year 2005 is very close to that of the climatological mean, which we estimate based on HALOE stratospheric methane measurements of the period 1994–2001. Assuming that one methane molecule forms 2 water molecules, the contribution from methane oxidation can be estimated from the difference between stratospheric and tropospheric methane concentration (see *Fueglistaler and Haynes* [2005] for details). It is known that the HALOE methane field may be biased in the vicinity of the tropopause of order 0.1 ppmv, and no reliable climatology of methane at very high latitudes can be obtained from HALOE. Hence, comparison of water vapor model results with observations has to take into account that there exists some uncertainty in the contribution from methane oxidation on the order of about 0.2 ppmv.

[30] For the comparison against measurements we prefer data from MLS (for validation see *Read et al.* [2007]) over those from HALOE because of the much higher sampling rate of the former and because of a dry bias of HALOE measurements [*Kley et al.*, 2000]. This restricts the comparison to model predictions from ERA-Interim only (there

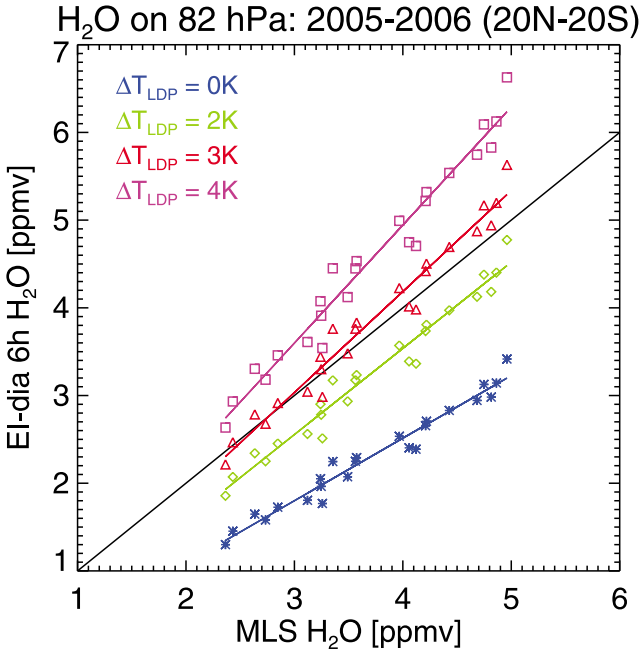

Figure 4. Observed versus modelled water vapor mixing ratios at 82 hPa (monthly means) for ERA-Interim diabatic trajectories over the period 2005–2006. Applied LDP temperature adjustment (see text) as labeled in Figure 4.

is no overlap between ERA-40 and MLS/Aura). However, comparison of results for TST for different years (not shown) shows that the differences shown in Figure 3 are robust, such that extending insights from comparison with observation from one model to the other is relatively straightforward.

4.2.1. The Dry Bias

[31] Stratospheric water vapor predictions based on methods very similar as employed here have been shown to yield good agreement with observations [*Fueglistaler et al.*, 2005; *Fueglistaler and Haynes*, 2005]. On the other hand, published results for shorter periods using slightly different input data [e.g., *Fueglistaler et al.*, 2004; *Bonazzola and Haynes*, 2004; *James et al.*, 2008; *Krüger et al.*, 2008] indicate differences in model predictions that have not been evaluated systematically before. Indeed, the calculations discussed here yield water vapor predictions that are consistently much drier than those of *Fueglistaler et al.* [2005]. Figure 4 shows the comparison of observed monthly mean water vapor concentrations by MLS/Aura at 82 hPa (20°S–20°N) and the corresponding model predictions based on EI-dia TST trajectories (blue symbols; other symbols discussed below). For this region, the TST fraction is very high, and methane oxidation is not important; in situ measurements show [e.g., *Volk et al.*, 1996; *Richard et al.*, 2006] methane levels at the tropical tropopause ~0.05 ppmv lower than in the troposphere; correspondingly the contribution to water vapor from methane oxidation arising from in-mixing of stratospherically old air is of order 0.1 ppmv, an order of magnitude smaller than the observed bias). Figure 4 shows that the bias is so large that a direct comparison with observations provides little insight.

[32] The differences between our results here and those of *Fueglistaler et al.* [2005] arise for a number of reasons. A straightforward reason is the use of different interpolation schemes in the vertical. The cubic-polynomial interpolation used here better captures the temperature minimum at the tropopause than a linear interpolation scheme as used in *Fueglistaler et al.* [2005]. The LDP temperature difference between linear and cubic-polynomial maximizes for trajectories passing the tropical tropopause (because of the large curvature of the temperature profile there), with the linearly interpolated values being on average about 0.5 K warmer. Further, ERA-40 is a little warmer at tropopause levels than ERA-Interim (further discussed below). However, as we will show below there are also other, more complex, factors that play a role.

[33] Given the large difference between observation and model prediction, questions about the usefulness of the model calculation may arise. Figure 4 shows that model predictions and observations (blue symbols) are not randomly distributed but in fact are highly correlated. Figure 4 also shows the model results obtained when an artificial, constant temperature correction of 2 K (green), 3 K (red), and 4 K (purple) is added to each trajectory's LDP temperature. Figure 4 shows that adding a constant correction of about 3 K to every LDP temperature is sufficient to bring model and observations to quite good agreement both in terms of mean and amplitude of seasonal variations. In other words, the model calculations suffer from a systematic bias that can be corrected quite well by one single, constant correction term. Note that this correction is introduced here without physical justification; it merely serves to make the point that the major deficit of the A-C paradigm seems to be a simple bias.

4.2.2. Comparison of Annual Mean Stratospheric Water Vapor Field

[34] Figure 5a shows the annual mean water vapor field (including contributions from methane and non-TST trajectories as described above and a constant LDP temperature adjustment of 3 K) based on the TST trajectories for the part of the stratosphere where the fraction of TST trajectories within 1 year is larger than 35% based on the EI-dia calculation (EI-kin and E40-dia give similar results). Note the hemispheric contrast in the overworld is a consequence of differences at entry alone and is not related to dehydration in the Antarctic vortex. Figure 5b shows the difference between the model prediction and observations. Throughout the stratospheric overworld, the differences between observations and model predictions are small (order ±10%). We note an alignment of the error structure with the pressure levels in potential-temperature space. This structure could arise from small errors in the estimation of the contribution from methane oxidation (HALOE methane has small biases near the tropopause), from the simplified treatment for non-TST trajectories, or from height-dependent differences in bias in the MLS measurements that are too small to be detected during validation. While the clear structure of the error in the overworld indicates that one should not discard it as insignificant, it is not clear that it is a consequence of an error in the model calculation of water entering the stratosphere. Hence, in the error budget presented below we keep this difference as an error term for the absolute accuracy of the calibration against the MLS/Aura data.

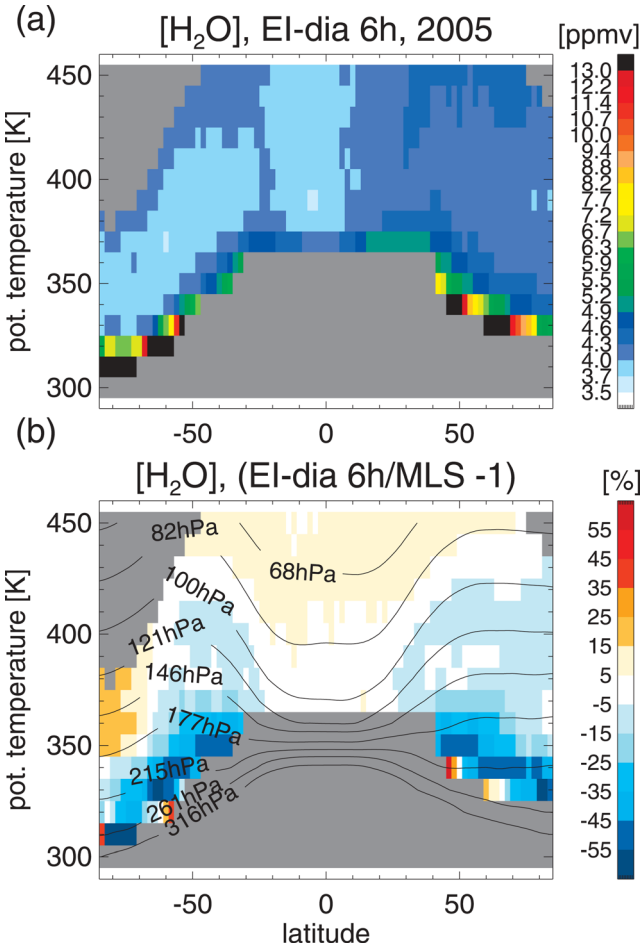

Figure 5. (a) The model water vapor field for 2005 based on ERA-Interim diabatic trajectories (EI-dia) for those regions where the TST fraction within 1 year is larger than 35%. Non-TST trajectories are assigned the annual mean entry mixing ratios determined from the equatorial TST trajectories at 400 K, adjusted for the drier conditions in 2004 (see Figure 6). Climatological mean contribution from methane oxidation is added based on an annual mean methane climatology from HALOE (polewards of 70° the profile at 60° is taken, leading to the possibility of a small dry bias). Note that dehydration in the polar vortices is explicitly not taken into account (see text). (b) Relative difference to MLS.

[35] Overall, however, the interpretation of Figure 5 is quite straightforward. From about 370 K the model calculation with a constant LDP temperature adjustment agrees well with observations despite the many simplifications. In contrast, the errors in the lowermost stratosphere, in particular along the extratropical tropopause, are larger, with a remaining dry bias of about 30%. This bias is smaller for the ERA-Interim kinematic calculation, while in the stratospheric overworld results are more similar. Because the processes controlling water vapor in the overworld and in the lowermost stratosphere are significantly different, we focus in the remainder of this paper on the overworld and defer analysis of the situation in the lowermost stratosphere to a follow-up publication.

5. Error Analysis in a Lagrangian Context

[36] The challenge presented by the results shown above is that differences in predicted water vapor arise from differences in the methodology to evaluate the advection-condensation paradigm, which constitute a serious obstacle to the assessment of the validity of the A-C hypothesis. In this section, we seek to establish a framework to evaluate and discuss sensitivities and "errors" in the Lagrangian frame of reference natural to the hypothesis. This will allow us to understand why model results differ and to assess the physical significance of differences between model and observations.

[37] Currently, there exists to our knowledge no theoretical framework that would allow calculation of errors in the predicted field from knowledge of errors in the Eulerian temperature field, wind field, and combination of the two. Fundamentally, the challenge is that the predicted field (water vapor) is evaluated from a threshold behavior, and consequently depends on a single position in space and time (the LDP) for each trajectory. Imperfect knowledge of temperature and winds can shift the LDP in time and position, and the resulting difference is not straightforward to calculate. In the following, we use a semiempirical approach that serves to set out the fundamental aspects of the problem and that provides sensible error estimates for stratospheric water vapor.

5.1. Two Case Studies

[38] As an additional motivation to understanding errors in a Lagrangian context, we first present two case studies. The first shows the impact of a temperature bias in the underlying temperature field, and the second the importance of small differences in transport relative to differences in the temperature fields of two data sets.

5.1.1. Case I

[39] Figure 6 shows the time series (2004–2009) of stratospheric water vapor mixing ratio anomalies (after subtracting out the mean annual cycle) at 82 hPa in the tropics (30°S–30°N) as measured by MLS/Aura, and the corresponding model predictions from kinematic, 1 year back-trajectories based on ERA-Interim with a constant adjustment of the LDP temperature as explained above, but without corrections for non-TST and methane. The point here is that the interannual variation of the modeled curve (red) and the measurements agree quite well but, in addition to shorter-term differences, there appears to be a drift between the observation (blue) and model prediction (red).

[40] Figure 6b shows the mean temperature error of ERA-Interim in a thin layer centered at 100 hPa as determined from a comparison with radiosondes (model minus observation, original data sampled twice per day; data derived from the ECMWF assimilation system). The data show ERA-Interim to be slightly cold biased up to 2007, with seasonal variations in the error. By the end of 2006, the mean bias decreases markedly, with generally better agreement between model and observations thereafter. This drift in temperatures is a consequence of the introduction of COSMIC GPS temperature data into the assimilation system

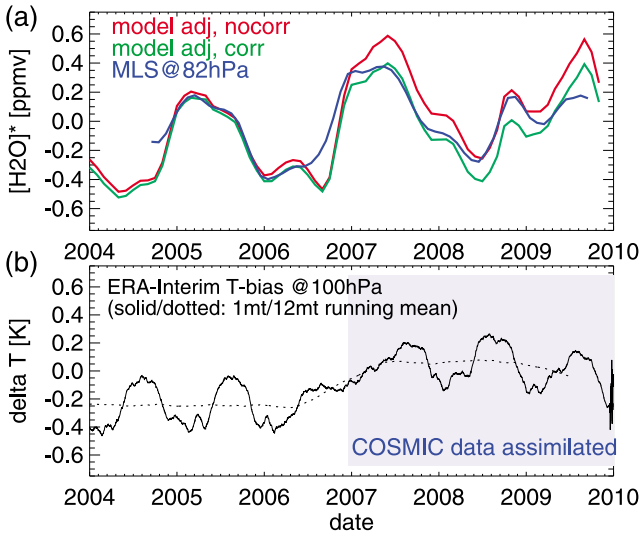

Figure 6. Water vapor mixing ratios observed by MLS/Aura at 82 hPa, averaged between 30°S and 30°N, and corresponding model results using ERA-Interim kinematic back-trajectories (integrated for 1 year in time). (a) The interannual anomalies (i.e., after subtracting the mean annual cycle) of MLS observations (blue), and the model calculations based on the raw ERA-Interim temperatures (red) and based on the bias-corrected ERA-Interim temperatures (green; see text for bias correction). Curves are smoothed with a 2-month running mean filter. Note that the model calculations require an adjustment of the LDP temperatures by about 3 K (see text). (b) The tropical mean temperature error of ERA-Interim (see text) smoothed with a 1 month (solid line, this is the correction as applied to the LDP temperature calculations shown above) and 12 month (dashed line) running-mean filter.

(D. Dee and A. Simmons, personal communication, 2009, 2010).

[41] As we have no information about the spatial structure of the temperature error at this point, we have constructed a simple correction for the known temperature error by adding the mean tropical temperature error (as function of pressure) onto the Lagrangian temperature history. From these temperature-corrected trajectories, stratospheric water vapor entry mixing ratios have been recalculated, giving the green line in Figure 6a. Figure 6a shows that this simple correction does not give perfect agreement with observations either, but does a fair job in removing the drift. This suggests that in this case the cause of the drift between the LDP model and observation indeed was the drift in the (ERA-Interim) temperature field that was used to calculate the Lagrangian dry points.

5.1.2. Case II

[42] Returning to the question of the relative importance of differences in pathways and underlying temperature field for the differences shown in Figure 3, we show in Figure 7 what happens when the temperature field used to determine the LDP temperature is swapped. That is, the temperature history along the trajectories is reevaluated using the ERA-Interim temperature field for ERA-40 trajectories and vice versa. This procedure allows us to some extent to disentangle effects of differences in the underlying temperature field and of differences in transport.

[43] Figure 7 shows the histogram of LDP temperatures for back-trajectories started at 400 K potential temperature between 10° S and 10°N, averaged over the year 2001. The two solid lines show the histogram where trajectory and temperature are taken from the same data set, and the dashed lines show the result when swapping the temperature field. Figure 7 shows that in this case the distributions are more similar for the cases with identical temperature data than identical pathway. Apparently, in this case the differences between the ERA-Interim and ERA-40 diabatic calculations are dominated by the differences in the ERA-40 and ERA-Interim temperature field. Further, the frequency distributions show that the differences between ERA-40 and ERA-Interim are due to a shift in the broad distribution and not due to, for example, the very cold outliers seen in ERA-Interim (i.e., at the tail of the distributions below 180 K). We have not been able to establish the origin of these extremely low temperatures (which are likely unrealistic given the model's resolution) in ERA-Interim, but it is reassuring to see that their impact on the LDP temperature distribution and mean is marginal.

5.2. Temperature Errors

[44] We have argued above that much of the difference between the two diabatic model calculations is the result of differences in the underlying temperature field. In the following, we wish to further quantify temperature-related errors and establish the relationship of Eulerian temperature errors and LDP temperature errors. First, we analyze the impact of spatially homogeneous temperature errors with a long characteristic time scale. In a second step, we discuss the impact of spatially inhomogeneous temperature errors both with long and short characteristic time scales.

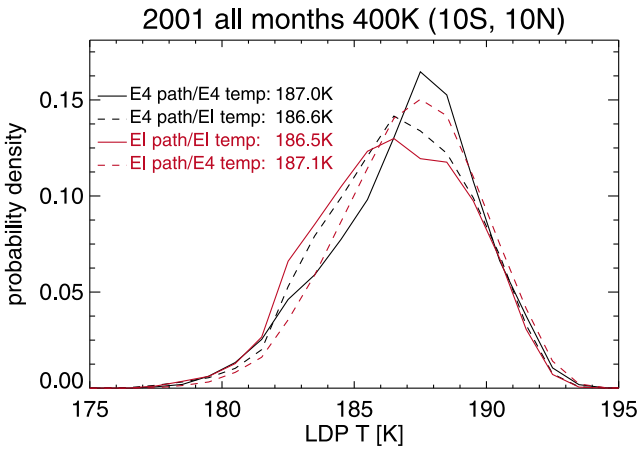

Figure 7. Histograms of the Lagrangian dry point temperatures for diabatic trajectories started at 400 K potential temperature between 10°S and 10°N based on ERA-Interim and ERA-40. Solid lines for matching temperatures and pathways (black: ERA-40; red: ERA-Interim), dashed lines for swapped temperature fields.

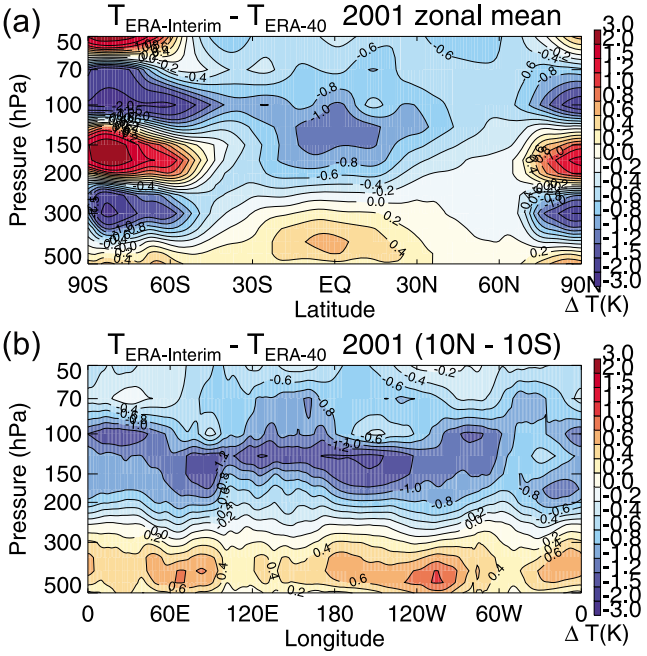

Figure 8. Temperature differences (year 2001); ERA-Interim minus ERA-40. (a) Zonal mean; (b) inner tropical mean.

5.2.1. Uniform Temperature Biases

[45] Figure 8 shows the annual mean (year 2001) difference between the (Eulerian) ERA-40 and ERA-Interim temperature fields. Figure 8 shows the zonal mean and inner tropical mean structure of ERA-Interim minus ERA-40. The zonal mean temperature difference is largest at high latitudes, where ERA-40 shows a well-known oscillatory temperature error (see *Fueglistaler et al.* [2009b]). In the upper troposphere, ERA-Interim is generally slightly warmer, and in the region of main interest here (upper tropical troposphere and stratosphere) ERA-Interim is colder than ERA-40. These differences peak at about 1 K slightly below the tropopause. The zonal structure (Figure 8b) shows that in general the temperature difference is zonally quite homogeneous, with maxima around the dateline.

[46] Figure 9 compares the Eulerian temperature difference to the corresponding Lagrangian difference. The Lagrangian difference is calculated from the Lagrangian cold point temperature profiles (calculated as the average LDP temperature in a pressure bin) of trajectories initialized above 380 K, and where the Lagrangian dry point is located between 10°S and 10°N. The solid line in Figure 9a shows the LDP temperature profile of the EI-dia model with temperatures from ERA-Interim, and the dashed line shows the temperature profile for the same trajectories, but now with the ERA-40 temperature data. Figure 9b shows the difference between the two Lagrangian calculations (dash-dotted line) and the Eulerian temperature difference in the same latitude range (dotted line). Comparison shows that the two profiles are quite similar, with the Lagrangian difference being ≤40% larger than the Eulerian difference. Because the Lagrangian dry point (on a given isentropic surface) is preferentially in regions of lowest temperatures [see *Bonazzola and Haynes*, 2004; *Fueglistaler et al.*, 2004, 2005], and the temperature differences between the two reanalyses happen to be largest (see Figure 8b) in the coldest region (over the western Pacific), the calculated larger difference for the Lagrangian case is not surprising.

[47] In this case the problem seems to be well behaved insofar as a time and area mean temperature correction (such as applied in the correction shown in Figure 6) does a good job in reconciling the water vapor predictions of the two calculations. However, the LDP distribution can change in pressure (as shown in Figure 9c), location and time in response to changes in the temperature field. In general, this coupling between temperature differences and LDP distribution (in space and time) differences cannot be accounted for with a uniform temperature correction, and we will return to this problem in section 5.2.2.

5.2.2. Nonuniform and Time-Varying Temperature Errors

[48] Lagrangian water vapor predictions are also sensitive to the variance (in both space and time) of temperature and errors therein, and it is this sensitivity which may be most challenging. Consider, for example, the case of a localized temperature bias. If the mean temperature field has a quasi-steady temperature structure as is the case for the TTL, the Lagrangian dry points are preferentially in regions of lower than average temperatures [*Fueglistaler et al.*, 2005]. In the case where the temperature bias is located in the coldest region, it would strongly affect the water vapor prediction, whereas it would do so only weakly if it were located in a warm region. Similar thought experiments can be carried out also for the impact of errors on various time scales. Specifically, if the time scale of the error is much shorter than the typical time scale of the air parcel in the vicinity of the LDP, we can predict its impact on water vapor from knowledge of the LDP and the error characteristics alone. Conversely, in the case where the error time scale is long, its effect on water vapor becomes

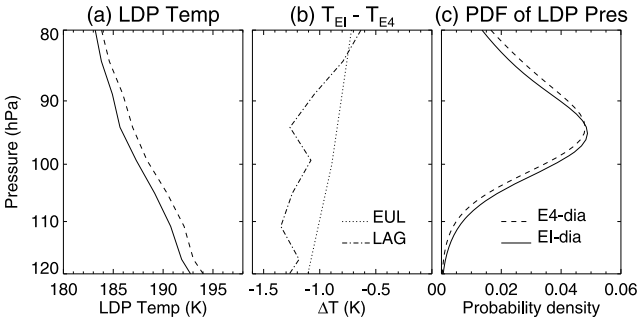

Figure 9. Temperature differences (year 2001); ERA-Interim minus ERA-40. (a) The Lagrangian dry point temperature profile determined from diabatic trajectories calculated with ERA-Interim, using ERA-Interim temperatures (solid) and ERA-40 (dashed) temperatures. (b) Difference of the two Lagrangian temperature profiles (as shown in Figure 9a) and the Eulerian temperature difference (dash-dotted and dotted lines). (c) Frequency distribution (profile) of the Lagrangian dry point of the ERA-Interim and ERA-40 calculations.

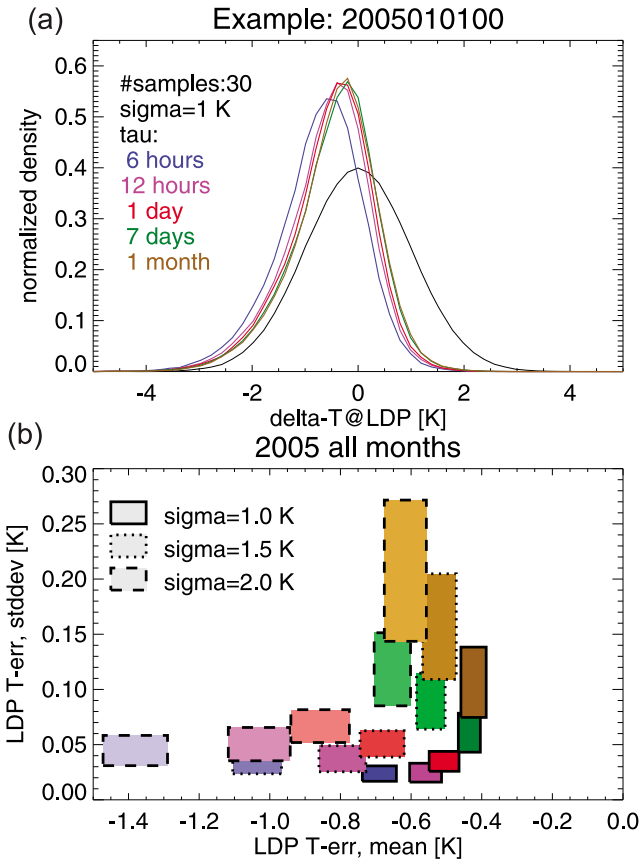

Figure 10. Estimate of the error in the Lagrangian dry point temperature due to a Gaussian-distributed temperature error. The error field employed here (see text) has a spatial scale of 30° longitude and 10° latitude and time scales ranging from τ_{err} = 6 h to 1 month, as labeled and color-coded. (a) Distribution of Eulerian temperature error with standard deviation of 1 K (black curve) that characterizes the Eulerian temperature error probability density distribution and the corresponding LDP temperature difference distributions (averaged over 30 different error history realizations). (b) The mean (x axis) and standard deviation (y axis) of the LDP temperature error in response to Gaussian error in the underlying T field. Calculations are based on Gaussian error distribution with standard deviations of 1, 1.5, and 2 K (solid, dotted, and dash-dotted lines; note associated variation in lightness), and the colors refer to the time scales as shown in Figure 10a. Mean and standard deviation are taken from an ensemble of back-trajectories started at a given time in the lower stratosphere. The calculations were carried out for 12 ensembles (started once per month in 2005), and the width and height of the "boxes" are the inter-ensemble standard deviation of LDP temperature mean error and standard deviation.

very difficult to predict as it may substantially change the time and position of the LDP.

[49] In order to characterize the impact of spatiotemporally varying temperature errors on water vapor in the situation considered here, we calculate the effect of random errors with a range of time scales. The temperature error is characterized as a sequence in time of two-dimensional (longitude/latitude) error fields, whereby a Gaussian random error is specified on a grid of 30° longitude by 10° latitude, with linear interpolation in between. The grid spacing therefore determines the spatial scale of the error field. Note that the chosen spacing seems a sensible choice for the specific problem considered here but might differ for the corresponding problem in the troposphere, for example. The time dependence is specified by changing the temperature error field after a time scale τ_{err}. These error fields are then superposed on the temperature history of the trajectories, and the LDP temperature distribution is recalculated. For every set of trajectories, the results shown represent the statistics of 30 different realizations of the error history.

[50] Figure 10a shows the change in the frequency distribution of the LDP temperature in response to a Gaussian temperature error with mean zero and standard deviation 1 K. Figure 10a shows that the result is sensitive to the time scale τ_{err}, with the largest effect for the shortest time scale (τ_{err} = 6 h). Figure 10b summarizes the results in terms of mean LDP temperature difference ("error") on the x axis and standard deviation between the 30 error history realizations on the y axis. The boxes show the parameter space populated by TST trajectories started on 400 K potential temperature once per month in 2005 (i.e., the size of the box is a measure for the variability due to seasonal variability in the characteristics of TST trajectories).

[51] Figures 10a and 10b shows that, as a general rule, an increase in temperature variance implies a negative bias in the LDP temperature (or, conversely, that underestimated variance yields a moist bias of the model calculation). Detailed discussion of the mathematics of the relation between Eulerian and Lagrangian errors is beyond the scope of this paper, but we note that according to Figure 10 the bias scales roughly linearly with the standard deviation in the Eulerian error field and that this scaling is expected to apply in general provided that the added variance is not so large as to change the nature of the LDP distribution.

[52] The increase in variance between different error realizations with increasing error time scale τ_{err} is also in agreement with expectations: As one approaches a quasi-stationary temperature error field, results are increasingly sensitive to the particular error field realisation if the LDP density distribution is inhomogeneous (as is the case here). Note that in the limit of very short time scales, the assumption of a Gaussian temperature error distribution becomes unphysical as the minimum temperature sampled in any time interval is unbounded. In this limit, the maximum temperature error sampled by the trajectory approaches the maximum amplitude of the process that produces the errors.

[53] Comparison of the temperature variance in twice-daily launched sondes at the tropical Pacific site Manus (2°S/147°E) of the Atmospheric Radiation Measurement (ARM) program with that of ERA-Interim at the nearest grid point shows an underestimation of variance in ECMWF. Around the tropical tropopause where the LDP density is highest, the standard deviation of the underestimation is about 0.5 K. The missing variance corresponds to a Gaussian distribution with about 1.5 K standard deviation.

[54] The error statistics for ERA-Interim show a standard deviation of about 1.5 K between all model-observation

differences at any given time (not shown; the time series of the mean error at 100 hPa is shown in Figure 6). This statistic does not allow us to say whether the error arises from over- or underestimation of variance in the model or from errors in the phase of temperature variations. In the latter case, the model could even have a correct temperature variance. Given that the standard deviation of temperature errors between different sounding locations at any given time is similar to the standard deviation of the missing temporal temperature variations at a single location (Manus) suggests that ERA-Interim indeed systematically underestimates temperature variance and that the missing variance is mainly on short time scales.

[55] From Figure 10 we see that for an underestimation of variance as suspected here (corresponding to a standard deviation of 1.5 K), the Lagrangian dry point temperatures are high biased by as much as 1 K. If the variance originated predominantly from gravity waves with short time scales, then the maximum error would essentially correspond to the amplitude of the wave. Incidentally, the amplitude of gravity waves in the layer of interest is also of order 1 K [see, e.g., *Wang et al.*, 2006; *Gary*, 2006; *Jensen et al.*, 2010], so a sensible (but arguably based on semiempirical considerations) estimate of the overall uncertainty from unresolved variability is about 1 ± 0.5 K.

[56] Hence, evaluation of the A-C paradigm based on ECMWF reanalysis data underestimates small-space-scale and short-time-scale temperature variance. The A-C paradigm is usually studied from a large-scale (synoptic) perspective, with the implicit "cloud parameterization" that condensate formed on resolved scales falls out completely, whereas that on unresolved scales does not fall out. The calculations of *Jensen and Pfister* [2004] show that indeed temperature variance related to gravity waves has a small net impact on water vapor concentrations, but the scale separation remains to be properly established (see *Fueglistaler and Baker* [2006] for discussion). Consequently, we calculate the error budget both with and without the effects of small-scale temperature perturbations not included in the ECMWF temperature field.

5.3. Errors in Transport

[57] Estimating the impact of erroneous transport on Lagrangian estimates of water vapor is even more challenging than the effects from temperature errors. From a conceptual standpoint, it may be sensible to differentiate transport errors as follows: (i) Systematic errors in the sense of either processes not resolved by the velocity field of the underlying model (e.g., individual convective cells in global-scale models) or systematic errors in the resolved flow or (ii) random errors, affecting, for example, the dispersion, a well-known problem for trajectories based on analyzed meteorological data.

[58] In the following we discuss the role of dispersion based on the differences between different methods to calculate vertical motion (i.e., kinematic versus diabatic trajectory calculations) and the role of the mean vertical velocity, which may be viewed as a case of systematic error in the transport.

5.3.1. Dispersion

[59] Figure 11 shows the annual average vertical dispersion of the four trajectory calculations, measured by the variance in potential temperature after 14 days of integration, with the variance calculated over the ensemble of trajectories ending at the same latitude and potential temperature.

[60] The two diabatic and the EI-kin calculations show a maximum in variance at the outflow levels of tropical deep convection, as may be expected (note that the variance is from backward trajectories; the corresponding picture for forward trajectories would look different). The two diabatic calculations further show larger variances in the stratosphere between about 30° and 60° latitude. These maxima are a consequence of the planetary wave activity over the extratropics moving air back and forth across the latitudinal gradient of radiative heating [see, e.g., *Sparling et al.*, 1997].

[61] Figure 11 shows that the dispersion is much larger in the entire domain for the kinematic trajectories based on ERA-40 than in any other model. This result is consistent with previously published results [e.g., *Schoeberl*, 2004; *Stohl et al.*, 2004; *Wohltmann and Rex*, 2008]. It is conceivable that some artificially enhanced dispersion is more realistic as a representation of the effect of small-scale mixing processes. However, the estimates of the diffusivity corresponding to the latter (e.g., *Legras et al.* [2003] estimate $D \approx 0.1\ \mathrm{m^2\ s^{-1}}$) are smaller than the diffusivity estimated for ERA-40 from the kinematic trajectories' dispersion by at least one order of magnitude. This argument therefore cannot justify the ERA-40 kinematic dispersion as realistic.

[62] The excessive dispersion of the ERA-40 kinematic becomes very obvious when looking at the situation in the extratropical stratosphere, where we have noted very high water mixing ratios well into the stratospheric overworld. Figure 12 shows the LDP distributions for trajectories ending in the extratropical overworld (beige shaded area) for E40-kin and E40-dia, separated into January/February and July/August. In the case of the Northern Hemisphere, summer situation (July/August), they typically experience their Lagrangian dry point at about the position of entry into the stratosphere in the tropics. However, in the case of the ERA-40 kinematic calculation, we find a large number of trajectories that experience their LDP between 340 K and 380 K, suggesting entry into the stratosphere at these subtropical locations and subsequent upward transport.

[63] This pathway is in contradiction with the sense of zonal mean diabatic circulation (recall that the red line in Figure 11 is the surface of zero radiative heating). In principle it might be allowed if there were zonal asymmetries in the radiative heating, but it would be manifested in chemical distributions, including the water vapor distribution. The strong differences between the shapes of the concentration contours in Figure 3a and those in Figure 1b indicate that this pathway is not important in reality.

[64] In the Southern Hemisphere, the LDP distribution of the E40-kin model shows a secondary maximum at high latitudes. Similarly to the Northern Hemisphere case, these trajectories may have entered the stratosphere quasi-isentropically, but in this case saturation mixing ratios at high latitudes are lower than at the position of entry into the stratosphere such that the LDP is in the area of the end positions.

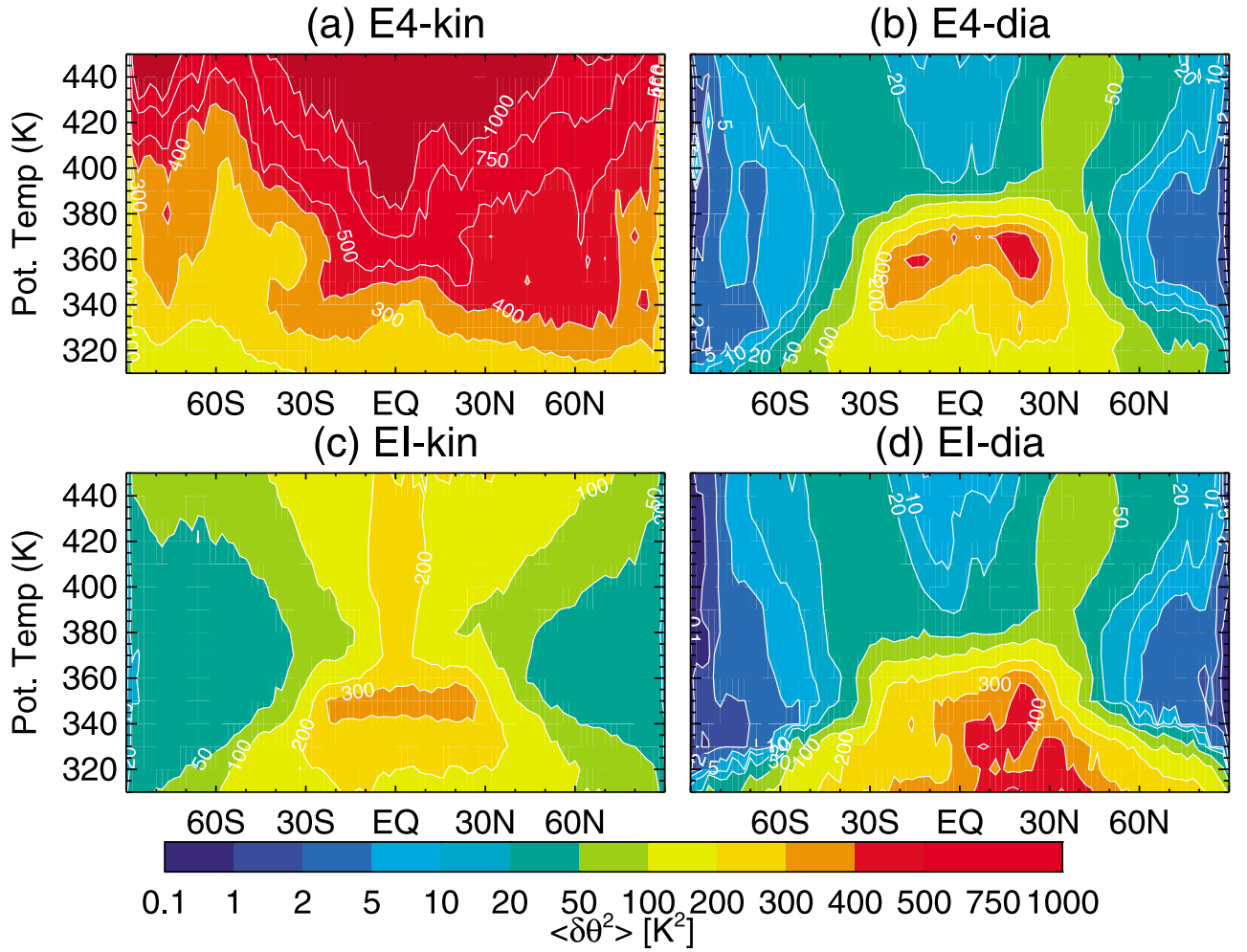

Figure 11. Annual mean (year 2001) dispersion in potential temperature of trajectories for the four models (as labeled in figure). Dispersion is calculated from variance in potential temperature change of trajectories started at given latitude/potential temperature and traced back for 14 days. Note that the illustrations show results for back-trajectories such that the layer of deep convective outflow shows up with large values.

[65] Interestingly, despite their large vertical dispersion the ERA-40 kinematic trajectories still reflect to some extent the strength of the transport barrier in the vicinity of the subtropical jet inasmuch as this spurious transport route is found mostly in the corresponding summer hemisphere (i.e., compare the JF and JA situations), where the transport barrier is weaker.

[66] Returning to Figure 11, we note that despite the large differences in dispersion, overall the LDP distributions in all model calculations are quite similar not only in latitude/height (as shown in Figure 12) but also in terms of their longitudinal position (not shown). This is even more so for trajectories ending in the stratospheric overworld at low latitudes (not shown). These trajectories have a lower probability to follow some (erroneous) path in the lowermost stratosphere and hence assume their LDP in the vicinity of the tropical tropopause irrespective of the dispersivity. Finally, from a practical point of view it is important that the kinematic calculation with ERA-Interim yields results fairly similar (except for the higher dispersion in the inner tropical stratospheric overworld) to those of the two diabatic trajectory calculations. The implication is that the newer model and the four-dimensional variational assimilation scheme of ERA-Interim yields a much less noisy vertical wind field such that ERA-Interim kinematic trajectory calculations are, from the point of view of water vapor predictions, of similar quality as those based on diabatic heating rates.

5.3.2. Mean Transport

[67] There exists an intrinsic dependence of the water vapor field on the time scales of atmospheric transport. On the one hand, as demonstrated in section 5.2.2, temporal fluctuations of the temperature field have an impact that depends on the relation between the time scale of the temperature fluctuation and that of transport. On the other hand, depending on the characteristics of the flow and temperature fields, the time scale of transport may have a significant impact on the resulting water vapor field. In the case of

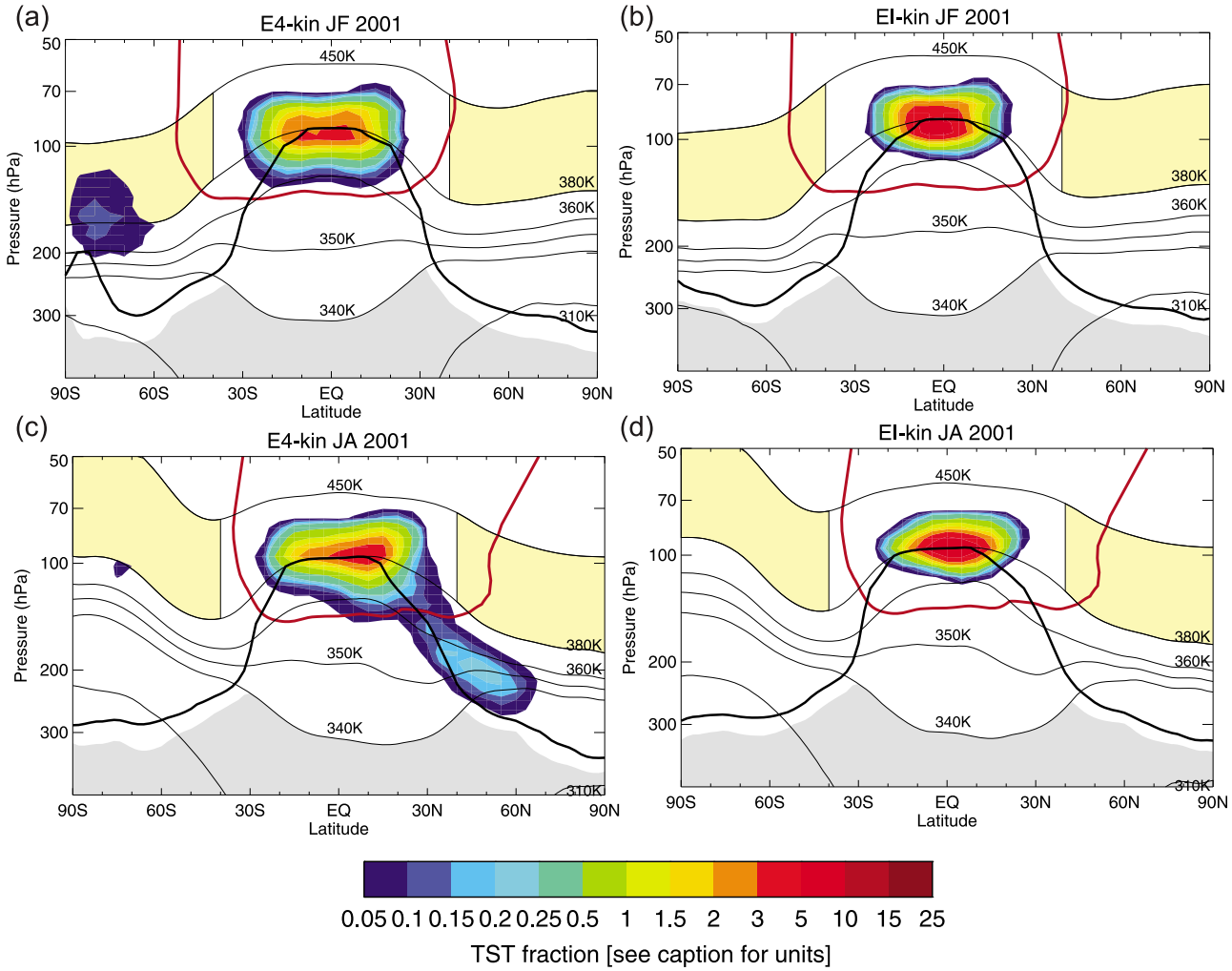

Figure 12. The Lagrangian dry point density distribution (color, in percentage of TST fraction per 5° latitude and 0.5 km log-pressure height) for trajectories started in the beige-shaded area (extratropical stratospheric overworld) where ERA-40 kinematic trajectories yield very high water vapor mixing ratios (see Figure 3). The black line shows the tropopause (as defined by 3 PVU or 380 K); the red line shows where clear the sky radiative heating is zero. The illustration shows the distributions separately for (a and b) January/February and (c and d) July/August for kinematic trajectories calculated using ERA-40 winds (Figures 12a and 12c) and ERA-Interim winds (Figures 12b and 12d). All results using diabatic heating rates (not shown) are very similar to those of the ERA-Interim kinematic calculations.

tropical TST where the horizontal structure of the temperature field at the tropopause plays an important role [see *Fueglistaler et al.*, 2005], the vertical (diabatic) velocity is of particular interest.

[68] Generally, the diabatic heating rates at the tropical tropopause in both ERA-40 and ERA-Interim are larger than those obtained from radiative transfer calculations using the detailed tracer profiles obtained from the Southern Hemisphere Additional Ozone Sounding (SHADOZ) program [see *Fueglistaler et al.*, 2009a, 2009b]. In order to explore the sensitivity of predicted water vapor to a bias in the mean upwelling, we have performed diabatic trajectory calculations based on the ERA-Interim data, whereby we have modified the radiative heating by a factor k ranging from 0.5 to 10. The latitudinally broad, fairly homogeneous structure of diabatic heating in the region of interest ensures that the observed effect mainly reflects the desired effect of modulation of the mean vertical velocity (as opposed to dispersion, which would be the case if the trajectories would experience quickly alternating, perhaps even positive/negative, heating rates).

[69] Figure 13a shows the LDP temperature of the TST ensemble for the four model calculations (year 2001) and their average transit times from the 360 K to the 400 K isentrope as a measure for the residence time in the region of minimum temperatures. As shown in section 5.2.1, the differences in LDP temperature between E40-dia and the two calculations based on ERA-Interim are mainly due to differences in the temperature fields of ERA-40 and ERA-Interim. Comparison of these three model calculations with the E40-kin model calculation, however, suggests that E40-kin is moister not only because of excessive dispersion but also because mean transit time may play a role as well. We note that the interpretation of the differences between the

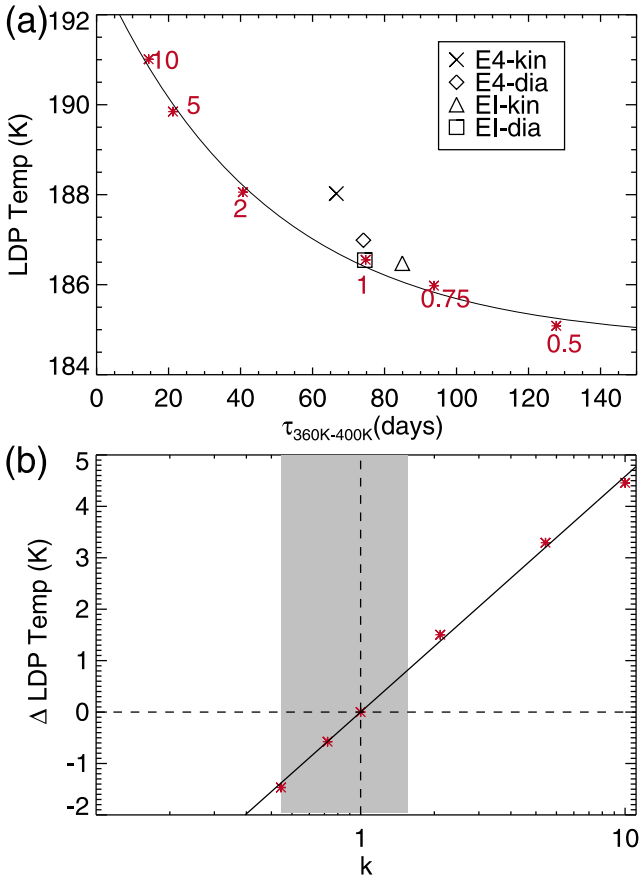

Figure 13. The impact of vertical velocity on water vapor entry mixing ratios, evaluated from TST trajectories (initialized once a month at 400 K potential temperature between 30°S and 30°N and with 1-year integration period; shown is the annual average for year 2001). (a) Average LDP temperature as function of transit time from 360 K to 400 K potential temperature, for all four models as labeled. Additionally, for EI-dia, radiative heating rates were artificially modified by multiplication with a factor k ($(D\theta/Dt)_{\mathrm{mod}} = k\,(D\theta/Dt)_{\mathrm{ECMWF}}$) ranging from 0.5 to 10 (red asterisks, labels indicate value of k). (b) The change in the average LDP temperature due to modification of radiative heating (i.e., as function of the factor k). The gray shading shows the ±50% range (see text).

four model calculations is also difficult because ensemble average transit time and ensemble average LDP temperature respond differently to integration period (not shown). In essence, increasing the trajectory integration period yields a larger change in transit time for kinematic trajectories exactly because of their larger dispersion. Conversely, the water vapor concentrations of both kinematic and diabatic trajectories change only a little (because the very long trajectories do not have a higher probability to cross the tropical tropopause at a location of higher than average temperature).

[70] The role of the mean transit time on stratospheric water vapor becomes clearer when looking at the results where we artificially modified the diabatic heating rates (the brown asterisks in Figure 13a, shown with a fitted exponential). They show a strong connection between upwelling time scale and resulting water vapor mixing ratios (expressed in terms of the mean LDP temperature).

[71] Figure 13b shows the change in average LDP temperature determined from 1 year back-trajectories as function of the modification of the diabatic heating rate, which can be interpreted as an uncertainty in the upwelling speed. The uncertainty in upwelling speed (as argued above and below) may be no larger than about 50% (shown as the gray shaded area), corresponding to an uncertainty in the LDP temperature of about 1 K.

[72] Estimates of ascent rates and transport time scales may be obtained also from tracer observations, but only few studies (e.g., analysis of CO_2 measurements by *Park et al.* [2007]) have focused on the layer of interest here (i.e., from about 360 K to 420 K potential temperature). An obvious reference to estimate ascent is the vertical propagation of the water vapor anomalies (the "tape recorder" signal [*Mote et al.*, 1996]). In general, the water vapor phase propagation is not only a function of mean ascent but also diffusion (see, e.g., *Hall et al.* [1999]; *Gregory and West* [2002]). In the region of interest here, the water vapor phase propagation is further affected by ongoing dehydration and possible hydration from very deep convection. Hence, instead of comparing derived quantities such as age of air, we directly compare the water vapor phase propagation of the model with that from observations.

[73] Figure 14 shows the anomalies (after subtraction of the annual mean profile) of tropical mean water vapor concentrations in the layer of interest for the year 2005. Comparison of the phase propagation (Figure 14c) between MLS/Aura (Figure 14a) and the water vapor field of EI-dia (Figure 14b) shows that both the ERA-Interim kinematic and diabatic trajectories capture the phase progression between 380 K and 450 K quite well. The agreement is worse for the calculation where radiative heating rates are brought into better agreement with the previously mentioned results (based on SHADOZ profiles using the Fu-Liou radiative transfer code) by a multiplication with a factor k = 0.5. Further, the slower ascent further worsens the agreement between observed and modelled water vapor by an additional bias of about 1 K (see Figure 13b). We note that different methods to determine the phase lag yield slightly different results. Using lagged correlation, instead of fitting with a sinusoidal of period 12 months as done here, suggests that the phase propagation based on the diabatic ERA-Interim trajectories is slightly too slow in the lower half (i.e., between 380 K and 420 K) of Figure 14c, as one would have suspected from visual comparison of Figures 14a and Figures 14b. Overall, however, the comparison suggests that the ERA-Interim trajectories capture the mean ascent without obvious bias.

[74] In the subsequent error calculation we will consider the model generated upwelling as the base case. A realistic error estimate for the mean ascent may be about ±20%, such that we use $k = 1 \pm 0.2$ in the error calculation below.

5.4. Overall Error Model for the Advection-Condensation Model

[75] In sections 5.2 and 5.3, we have explored the sensitivity of results to uncertainties in the temperature field and

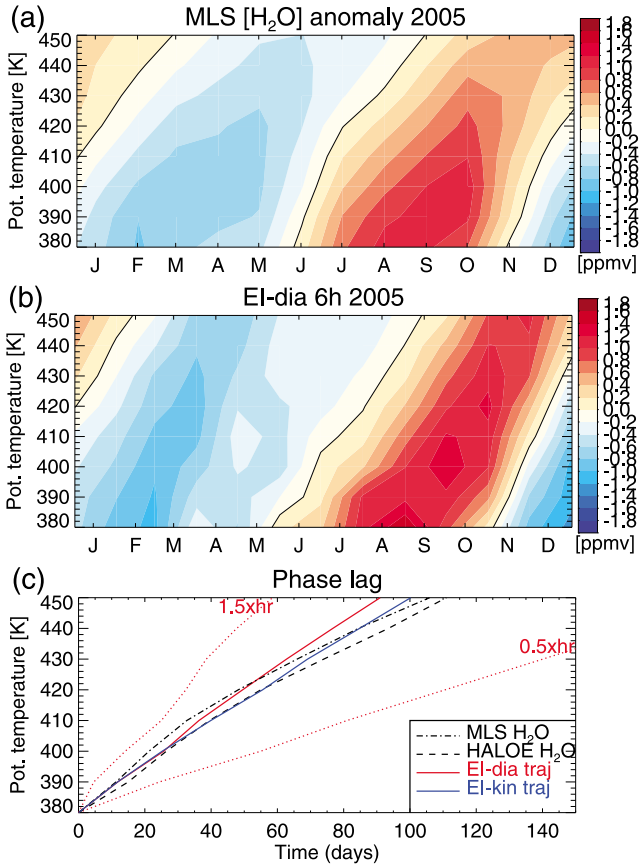

Figure 14. (a) Tropical mean (10°S–10°N) water vapor mixing ratio anomalies (after subtraction of annual mean) from MLS/Aura measurements in 2005. (b) Tropical mean (10°S–10°N) water vapor mixing ratio anomalies (after subtraction of annual mean) from model calculation EI-dia, with 1 year integration period. (Calculations use an adjustment of the LDP temperature of order 3 K, see text.) (c) Phase propagation (phase determined from fit with sinusoidal with period 12 months) for measurements from MLS/Aura (year 2005; dash-dotted line) and HALOE/UARS (climatology; dashed line). Model calculations are based on ERA-Interim 1 year kinematic (blue solid line) and diabatic (red solid line) back-trajectories; dotted red lines show results for multiplication of the diabatic heating rates (see text) by a factor $k = 0.5$ (slower ascent) and $k = 1.5$ (faster ascent).

circulation. Here, we present an error budget (based on the sources of error identified in this paper) for water vapor predictions for the stratospheric overworld, which is simpler than for the lowermost stratosphere.

[76] Let us write the total error of the Lagrangian dry point (ϵ_{LDP}) as the sum (note that the errors are only approximately additive) of the time and area mean temperature error of the model in the region of interest ($\epsilon_{T-bias,model}$), the error in the temperature variance of the model in the area of interest ($\epsilon_{T-var,model}$), the error arising from an error in the mean transport time scale ($\epsilon_{circ-bias}$), and the error from errors in the dispersion ($\epsilon_{circ-var}$):

$$\epsilon_{LDP} = \epsilon_{T-bias,model} + \epsilon_{T-var,model} + \epsilon_{circ-bias} + \epsilon_{circ-var}. \quad (1)$$

[77] Table 1 summarizes the errors for calculations based on ERA-Interim. We can then calculate the difference between observation (expressed as frost point temperature, $T^{frost}_{observed}$) and model prediction

$$\epsilon_{A-C} = T^{frost}_{observed} - (T_{LDP} + \epsilon_{LDP}), \quad (2)$$

which is the error in the prediction arising from the underlying assumptions of the A-C paradigm.

5.5. Quantification of Processes Neglected by the A-C Paradigm

[78] Figure 15 shows the required LDP temperature adjustment that yields best agreement with MLS/Aura observations at 82 hPa and 20°S–20°N for each month between start of measurements in 2004 and end of 2009 for 1 year diabatic and kinematic trajectories based on ERA-Interim. Figure 15 shows that the required adjustment is of order 3 K (as already seen in Figure 4 for the calculations using a fixed LDP temperature correction), with the difference between kinematic and diabatic trajectories prior to 2007 being of similar order as those found for the 5-month trajectories in 2001 (Figure 3). For the kinematic calculations, the difference between the two periods (decreasing from 3.1 K to 2.7 K) is broadly consistent with the mean shift of the ERA-Interim temperatures end of 2007 due to the assimilation of COSMIC GPS temperature data (as shown in Figure 6). Conversely, the LDP temperature based on the diabatic trajectories does not show a decrease. Although this different behavior should not be overrated (the difference is about −0.25 K in

Table 1. Error Terms for Estimate of Water Vapor in the Stratospheric Overworld for Calculations Using ERA-Interim Data[a]

Error	Bias (K)	σ (K)	Estimate Based On
$\epsilon_{T-calib}$	0.0	±0.4	Calibration against MLS/Aura (calib. location and uncertainty of HALOE CH4).
$\epsilon_{T-bias-0406}$	−0.25	±0.2	ERA-Interim temperature statistics for 2004–2006; see Figure 6.
$\epsilon_{T-bias-0709}$	0.0	±0.2	ERA-Interim temperature statistics for 2007–2009; see Figure 6.
$\epsilon_{T-var-syn}$	0.0	±0.5	Variance on synoptic scale ok, possible quasi-stationary spatially inhomogeneous biases, see section 5.2.2.
$\epsilon_{T-var-meso}$	+1.0	±0.5	Variance on mesoscale too small (GW), LDP temperature estimates are high biased; see section 5.2.2.
$\epsilon_{circ-bias}$	0.0	±0.5	Uncertainty in vertical ascent order 20% (see Figure 14c), conversion to T error see Figure 13b.
$\epsilon_{circ-var}$	0	±0.1 K	Dispersion for EI, based on difference EI-kin to EI-dia, Figure 13a.

[a]Results are expressed as frost point temperatures.

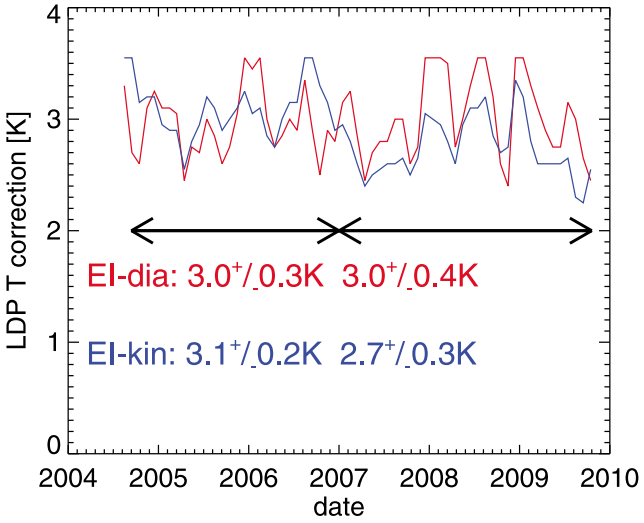

Figure 15. Time series of monthly mean adjustment to Lagrangian dry point temperature required to bring model predictions in agreement with MLS/Aura observations between 20°S and 20°N at 82 hPa. Trajectories are 1 year back-trajectories started every 10 days (kinematic: blue; diabatic: red) based on ERA-Interim data. Values given are the mean and standard deviation over the periods indicated by the black arrows.

the Eulerian perspective, which is less than the standard deviation of the difference between model and observation), it exemplifies that diabatic trajectories are not necessarily superior per se. The model's diabatic heat budget is not constrained by the assimilation process [see *Fueglistaler et al.*, 2009b] and, for example, a drift in the assimilated temperature field not only changes the saturation mixing ratio field but also introduces a change in the model's longwave radiative heating rates, which in turn affects residence times and consequently water vapor mixing ratios (as shown in Figure 13).

[79] Figure 16a shows the required LDP temperature adjustment (separately for the period 2004–2006 and 2007–2009) for the kinematic and diabatic trajectory calculations. Figure 16b shows the expected total model error (from Table 1), whereby we have separated the error calculation (using standard error propagation) into mesoscale and synoptic-scale perspective (i.e., taking the corresponding values for ϵ_{T-var} from Table 1).

[80] Figure 16c shows our estimate of the error ϵ_{A-C} arising from the assumption underlying the A-C paradigm. Figure 16 shows that after taking into account the uncertainties in the method, all scenarios have a substantial dry bias. A rough translation from temperature error to relative water vapor mixing ratio error gives for 1 K a 14% water change (assuming a mean entry mixing ratio of 3.5 ppmv and a sensitivity of the water vapor saturation mixing ratio of 0.5 ppmv/K; see *Fueglistaler and Haynes* [2005]). Evaluation the A-C paradigm from a synoptic-scale perspective yields a residual dry bias of about −40% ± 10% in water vapor mixing ratio. Taking into account unresolved mesoscale temperature variability increases the dry bias to about −50% ± 10%.

6. Discussion and Outlook

[81] We have analyzed the case of stratospheric water vapor from the perspective of the advection-condensation paradigm. We have shown previously that this approach works very well for stratospheric water vapor [*Fueglistaler et al.*, 2005] and provides a sensible explanation for observed interannual variability and trends [*Fueglistaler and Haynes*, 2005]. In this work, we present the first systematic and comprehensive analysis of the impact of uncertainties in temperatures and transport on water vapor predictions based on the A-C paradigm. We observe significant differences between different model calculations and a consistent dry bias except in calculations based on ERA-40 kinematic

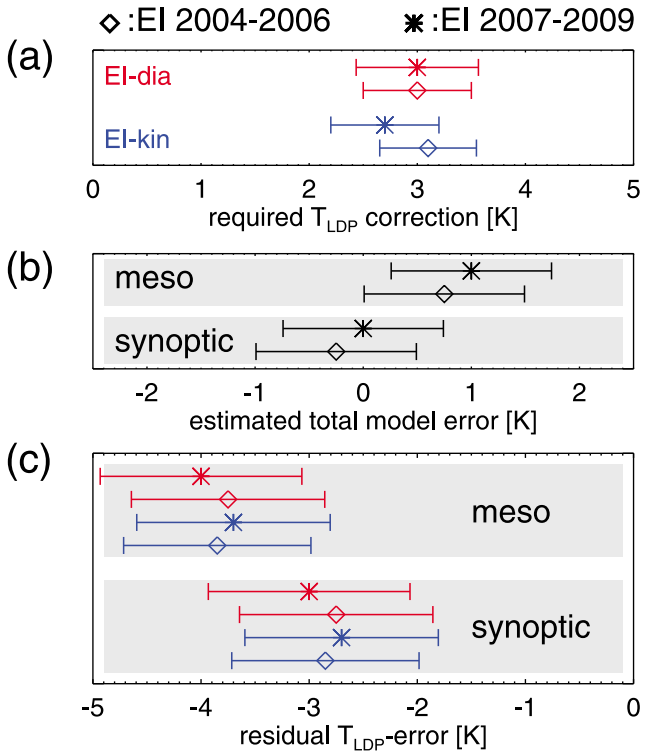

Figure 16. Error calculation for the stratospheric overworld for estimates of the tropical (20°S–20°N; narrow band to reduce potential impact from methane oxidation) water vapor at 82 hPa. (a) The required average (separately for the periods 2004–2006 and 2007–2009, indicated with diamonds and asterisks) LDP temperature adjustment to bring model results (blue: kinematic, red diabatic) in agreement with MLS/Aura measurements. (b) Error of LDP temperature based on equation (1) and values listed in Table 1 using standard error propagation. Calculation separately for mesoscale (i.e., with gravity waves) and synoptic-scale perspective (i.e., without gravity waves) (as labeled). (c) The difference between required adjustment and LDP error estimate, interpreted as residual unexplained by the advection/condensation model for kinematic and diabatic model calculations, with/without mesoscale temperature fluctuations considered.

trajectories. Consequently, interpretation of differences (or agreement) between A-C model predictions and observations in terms of the effect of process deliberately neglected in the approach requires an adequate error calculation in the Lagrangian frame of reference. We have introduced a semiempirical approach for this error calculation for the case of the stratospheric overworld.

[82] Taking model uncertainties into account, we find that water vapor predictions based on the A-C paradigm have a dry bias of about −40% ± 10%, and −50% ± 10% when mesoscale temperature variability unresolved by ERA-Interim is taken into account. Remarkably, a single (constant in time and location) correction of the LDP temperature restores not only the correct annual mean water vapor mixing ratios but also the predictive power of the LDP estimates for seasonal and interannual variability. Hence, the A-C paradigm seems to capture the leading-order process that controls stratospheric water vapor, but the cause of the dry bias requires further attention.

[83] The assumption of instantaneous and complete dehydration to the minimum saturation mixing ratio inevitably overestimates dehydration. We expect the following processes would contribute to correcting the dry bias. First, for in situ formed cirrus clouds the possible presence of a nucleation barrier and incomplete fallout of the condensate both lead to higher water vapor mixing ratios than expected from the LDP. The model study of *Jensen and Pfister* [2004] quantifies the contribution from these processes to 10–40% of the minimum saturation mixing ratio, which agrees quite well with the dry bias diagnosed in this study. Second, the evaporation of condensate detraining from deep convection [*Schiller et al.*, 2009, and references therein] will lead to a moistening that is not included in our model calculations. Significant methodological difficulties have prevented upscaling of this latter effect from single observation to the global scale, and, indeed, measured temporal variability in the isotopic depletion of stratospheric water [*Notholt et al.*, 2010; *Steinwagner et al.*, 2010] shows remarkably little signature that could be linked directly to convection.

[84] The results presented in this study will serve as a much-needed backdrop against which moistening effects from evaporating condensate can be studied for the case of troposphere-to-stratosphere transport of water vapor. Further, the large uncertainty found here inherent to the method to evaluate the A-C paradigm should motivate similar attempts for rigorous quantification of the validity of the paradigm in the troposphere.

[85] **Acknowledgments.** We thank Dick Dee and Adrian Simmons (ECMWF) for providing ERA-Interim temperature error statistics. Y.S.L. was supported by a NERC PhD studentship as part of the ACTIVE consortium project. S.F. was supported by a NERC Advanced Fellowship. Finally, we thank three anonymous reviewers for their careful and constructive reviews.

References

Bonazzola, M., and P. H. Haynes (2004), A trajectory-based study of the tropical tropopause region *J. Geophys. Res.*, *109*, D20112, doi:10.1029/2003JD004356.

Brewer, A. W. (1949), Evidence for a world circulation provided by the measurements of helium and water vapor distribution in the stratosphere, *Q. J. R. Meteorol. Soc.*, *75*, 351–363.

Fueglistaler, S., and M. B. Baker (2006), A modelling study of the impact of cirrus clouds on the moisture budget of the upper troposphere, *Atmos. Chem. Phys.*, *6*, 1425–1434.

Fueglistaler, S., and P. H. Haynes (2005), Control of interannual and longer-term variability of stratospheric water vapor, *J. Geophys. Res.*, *110*, D24108, doi:10.1029/2005JD006019.

Fueglistaler, S., H. Wernli, and T. Peter (2004), Tropical troposphere-to-stratosphere transport inferred from trajectory calculations, *J. Geophys. Res.*, *109*, D03108, doi:10.1029/2003JD004069.

Fueglistaler, S., M. Bonazzola, P. H. Haynes, and T. Peter (2005), Stratospheric water vapor predicted from the Lagrangian temperature history of air entering the stratosphere in the tropics, *J. Geophys. Res.*, *110*(D8), D08107, doi:10.1029/2004JD005516.

Fueglistaler, S., A. Dessler, T. Dunkerton, I. Folkins, Q. Fu, and P. W. Mote (2009a), Tropical tropopause layer, *Rev. Geophys.*, *47*, RG1004, doi:10.1029/2008RG000267.

Fueglistaler, S., B. Legras, A. Beljaars, J.-J. Morcrette, A. Simmons, A. M. Tompkins, and S. Uppala (2009b), The diabatic heat budget of the upper troposphere and lower/mid stratosphere in ECMWF reanalyses, *Q. J. R. Meteorol. Soc.*, *135*, 21–37, doi:10.1002/qj.361.

Galewsky, J., A. Sobel, and I. Held (2005), Diagnosis of subtropical humidity dynamics using tracers of last saturation, *J. Atmos. Sci.*, *62*, 3354–3367.

Gary, B. L. (2006), Mesoscale temperature fluctuations in the stratosphere, *Atmos. Chem. Phys.*, *6*, 4577–4589.

Gregory, A. R., and V. West (2002), The sensitivity of a model's stratospheric tape recorder to the choice of advection scheme, *Q. J. R. Meteorol. Soc.*, *128*, 1827–1846.

Hall, T. M., D. W. Waugh, K. A. Boering, and R. A. Plumb (1999), Evaluation of transport in stratospheric models, *J. Geophys. Res.*, *104*, 18,815–18,839, doi:10.1029/1999JD900226.

Haynes, P., and E. Shuckburgh (2000), Effective diffusivity as a diagnostic of atmospheric transport. 2. Troposphere and lower stratosphere, *J. Geophys. Res.*, *105*(D18), 22,795–22,810.

Holton, J. R., P. H. Haynes, M. E. McIntyre, A. R. Douglass, R. B. Rood, and L. Pfister (1995), Stratosphere-troposphere exchange, *Rev. Geophys.*, *33*, 403–439.

Hoskins, B. J. (1991), Toward a PV-theta view of the general circulation, *Tellus, Ser. A*, *43*, 27–35.

Immler, F., K. Krüger, S. Tegtmeier, M. Fujiwara, P. Fortuin, G. Verver, and O. Schrems (2007), Cirrus clouds, humidity, and dehydration in the tropical tropopause layer observed at Paramaribo, Suriname (5.8N, 55.2W), *J. Geophys. Res.*, *112*, D03209, doi:10.1029/2006JD007440.

James, R., M. Bonazzola, B. Legras, K. Surbled, and S. Fueglistaler (2008), Water vapor transport and dehydration above convective outflow during Asian monsoon, *Geophys. Res. Lett.*, *35*, L20810, doi:10.1029/2008GL035441.

Jensen, E., and L. Pfister (2004), Transport and freeze-drying in the tropical tropopause layer, *J. Geophys. Res.*, *109*, D02207, doi:10.1029/2003JD004022.

Jensen, E. J., L. Pfister, T.-P. Bui, P. Lawson, and D. Baumgardner (2010), Ice nucleation and cloud microphysical properties in tropical tropopause layer cirrus, *Atmos. Chem. Phys.*, *10*, 1369–1384.

Kley, D., et al. (2000), SPARC Assessment of upper tropospheric and stratospheric water vapour, *WCRP 113, WMO/TD No. 1043, SPARC Rep. No. 2*, World Meteorol. Organ., Geneva.

Krüger, K., S. Tegtmeier, M. Rex (2008), Long-term climatology of air mass transport through the Tropical Tropopause Layer (TTL) during NH winter, *Atmos. Chem. Phys.*, *8*, 813–823.

Lambert, A., et al. (2007), Validation of the Aura Microwave Limb Sounder middle atmosphere water vapor and nitrous oxide measurements, *J. Geophys. Res.*, *112*, D24S36, doi:10.1029/2007JD008724.

Legras, B., B. Joseph, and F. Lefévre (2003), Vertical diffusivity in the lower stratosphere from Lagrangian back trajectory reconstructions of ozone profiles, *J. Geophys. Res.*, *108*(D18), 4562, doi:10.1029/2002JD003045.

Liu, Y. (2009), Lagrangian studies of troposphere-to-stratosphere transport, Ph.D dissertation, University of Cambridge, 134 pp., Available at http://www.atm.damtp.cam.ac.uk/people/yl238/thesis.pdf.

Methven, J. (1997), Offline trajectories: Calculation and accuracy, U.K. University Global Atmos. Modelling Programme 44.

Methven, J., S. R. Arnold, F. M. O'Connor, H. Barjat, K. Dewey, J. Kent, and N. Brough (2003), Estimating photochemically produced ozone throughout a domain using flight data and a Lagrangian model, *J. Geophys. Res.*, *108* (D9), 4271, doi:10.1029/2002JD002955.

Mote, P. W., K. H. Rosenlof, M. E. McIntyre, E. S. Carr, J. C. Gille, J. R. Holton, J. S. Kinnersley, and H. C. Pumphrey (1996), An atmospheric tape recorder: The imprint of tropical tropopause temperatures on stratospheric water vapor, *J. Geophys. Res.*, *101*, 3989–4006.

Notholt, J., G. C. Toon, S. Fueglistaler, P. O. Wennberg, F. W. Irion, M. McCarthy, M. Scharringhausen, T. Siek Rhee, A. Kleinbohl, and V. Velazco (2010), Trend in ice moistening the stratosphere: Constraints from isotope data of water and methane, *Atmos. Chem. Phys.*, *10*, 201–207.

Park, S., et al. (2007), The CO_2 tracer clock for the Tropical Tropopause Layer, *Atmos. Chem. Phys.*, *7*, 3989–4000.

Pierrehumbert, R. T., and R. Roca (1998), Evidence for control of Atlantic subtropical humidity by large scale advection, *Geophys. Res. Lett.*, *25* (24), 4537–4540.

Read, W. G., et al. (2007), Aura Microwave Limb Sounder upper tropospheric and lower stratospheric H2O and relative humidity with respect to ice validation, *J. Geophys. Res.*, *112*, D24S35, doi:10.1029/2007JD008752.

Richard, E. C., et al. (2006), High-resolution airborne profiles of CH_4, O_3 and water vapor near tropical Central America in late January to early February 2004, *J. Geophys. Res.*, *111*, D13304, doi:10.1029/2005JD006513.

Schiller, C., J.-U. Grooss, P. Konopka, F. Plöger, F. H. Silva dos Santos, and N. Spelten (2009), Hydration and dehydration at the tropical tropopause, *Atmos. Chem. Phys.*, *9*, 9647–9660.

Schoeberl, M. R. (2004), Extratropical stratosphere-troposphere mass exchange, *J. Geophys. Res.*, *109*, D13303, doi:10.1029/2004JD004525.

Simmons, A., S. Uppala, D. Dee, and S. Kobayashi (2006), ERA-Interim: New ECMWF reanalysis products from 1989 onwards, *ECMWF Newslett.*, *110*, 25–35.

Sparling, L. C., J. A. Kettleborough, P. H. Haynes, M. E. McIntyre, J. E. Rosenfield, M. R. Schoeberl, and P. A. Newman (1997), Diabatic cross-isentropic dispersion in the lower stratosphere, *J. Geophys. Res.*, *102*(D22), 25,817–25,829.

Steinwagner, J., S. Fueglistaler, G. Stiller, T. von Clarmann, M. Kiefer, P. P. Boorsboom, A. van Delden, and T. Rockmann (2010), Tropical dehydration processes constrained by the seasonality of stratospheric deuterated water, *Nat. Geosci.*, *3*, 262–266, doi:10.1038/NGEO822.

Stohl, A., O. Cooper, and P. James (2004), A cautionary note on the use of meteorological analysis fields for quantifying atmospheric mixing, *J. Atmos. Sci.*, *61*, 12, 1446–1453.

Uppala, S. M., et al. (2005), The ERA-40 re-analysis, *Q. J. R. Meteorol. Soc.*, *131*, 2961–3012.

Uppala, S. M., D. Dee, S. Kobayashi, P. Berrisford, and A. Simmons (2008), Towards a climate data assimilation system: Status update of ERA-Interim, *ECMWF Newslett.*, *115*, 12–18.

Volk, C. M., et al. (1996), Quantifying transport between the tropical and mid-latitude lower stratosphere, *Science*, *272*(5269), 1763–1768.

Wang, L., M. J. Alexander, T. P. Bui, and M. J. Mahoney (2006), Small-scale gravity waves in ER-3 MMS/MTP wind and temperature measurements during CRYSTAL-FACE, *Atmos. Chem. Phys.*, *6*, 1091–1104.

Wohltmann, I., and M. Rex (2008), Improvement of vertical and residual velocities in pressure or hybrid sigma-pressure coordinates in analysis data in the stratosphere, *Atmos. Chem. Phys.*, *8*, 265–272.

Wright, J. S., A. Sobel, and J. Galewsky (2010), Diagnosis of zonal mean relative humidity changes in a warmer climate, *J. Clim.*, *23*, 4556–4569.

S. Fueglistaler, Department of Geosciences, Princeton University, Princeton, NJ 08544-1003, USA. (stf@princeton.edu)

P. H. Haynes, Department of Applied Mathematics and Theoretical Physics, University of Cambridge, Wilberforce Road, Cambridge CB3 0WA, UK.

Y. S. Liu, School of Mathematics and Statistics, University of St Andrews, North Haugh, Saint Andrews KY16 9SS, UK. (yliu@mcs.st-and.ac.uk)